

---

# Evaluating Generative Models Using Divergence Frontiers

---

Josip Djolonga\*

Mario Lucic

Marco Cuturi

Olivier Bachem

Olivier Bousquet

Sylvain Gelly

Google Research, Brain Team

## Abstract

Despite the tremendous progress in the estimation of generative models, the development of tools for diagnosing their failures and assessing their performance has advanced at a much slower pace. Recent developments have investigated metrics that quantify which parts of the true distribution are modeled well, and, on the contrary, what the model fails to capture, akin to precision and recall in information retrieval. In this paper, we present a general evaluation framework for generative models that measures the trade-off between precision and recall using Rényi divergences. Our framework provides a novel perspective on existing techniques and extends them to more general domains. As a key advantage, it allows for efficient algorithms that are directly applicable to continuous distributions directly without discretization. We further showcase the proposed techniques on a set of image synthesis models.

## 1 Introduction

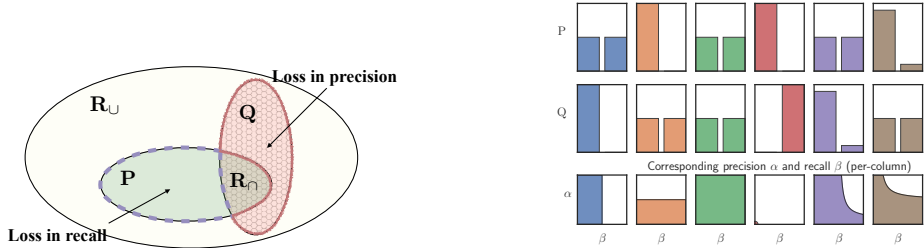
Deep generative models, such as generative adversarial networks [5] and variational autoencoders [7, 18], have recently risen to prominence due to their ability to model high-dimensional complex distributions. While we have witnessed a tremendous growth in the number of proposed models and their applications, a comprehensive set of quantitative evaluation measures is yet to be established. Obtaining sample-based quantities that can reflect common issues occurring in training generative models, such as “mode dropping” (failing to adequately capture all the modes of the target distribution) or “oversmoothing” (inability to produce the high frequency characteristics of points in the true distribution) remains a key research challenge.

Currently used metrics, such as the inception score (IS) [21] and the Fréchet inception distance (FID) [6] produce single number summaries quantifying the goodness of fit. Thus, even though they can detect poor performance, they cannot shed light into the underlying cause. Recently, Sajjadi et al. [20] and later Kynkäänniemi et al. [8] have offered an alternative view, motivated by the notions of precision and recall in information retrieval. Intuitively, the precision captures the average “quality” of the generated samples, while the recall measures how well the target distribution is covered. It was demonstrated that such metrics can disentangle these two common failure modes.

Unfortunately, these recent approaches rely on data quantization and do not provide a theory that can be directly used on with continuous distributions. For example, in [20] the data is first clustered and then the resulting class-assignment histograms are compared. In [8] the space is covered with hyperspheres and is only sensitive to the size of the overlap of the supports of the distributions.

---

\*Correspondence to Josip Djolonga (josipd@google.com) and Mario Lucic (lucic@google.com).



(a) When  $P$  and  $Q$  are uniform we can define natural precision and recall concepts using  $R_{\cup}$  and  $R_{\cap}$ , which are uniform on the union and intersection of the supports of  $P$  and  $Q$  respectively. (b) Examples with categorical  $P$  and  $Q$ , reproduced from [20].

Figure 1: For uniform measures we can define natural concepts using set operation (a). Similarly, when they are simple categorical distributions, we would like to generate curves like those in (b).

In this work, we present an evaluation framework based on the Pareto frontiers of Rényi divergences that encompasses these previous contributions as special cases. Beyond this novel perspective on existing techniques, we provide a general characterization of these Pareto frontiers, in both the discrete and continuous case. This in turn enables efficient algorithms that are directly applicable to continuous distributions without the need for discretization.

**Contributions** (1) We propose a general framework for comparing distributions based on the Pareto frontiers of statistical divergences. (2) We show that the family of Rényi divergences are particularly well suited for this task and derive curves that can be interpreted as precision-recall tradeoffs. (3) We develop tools to compute these curves for several widely used families of distributions. (4) We show that the recently popularized definitions of precision and recall correspond to specific instances of the proposed framework [20, 8]. In particular, we give a theoretically sound geometric interpretation of the definitions and algorithms in [20, 8]. (5) We showcase the utility of the proposed framework by applying it to state-of-the-art deep generative models.

## 2 Precision-Recall Tradeoffs for Generative Models

The central problem considered in the paper is the development of a framework that formalizes the concepts of precision and recall for arbitrary measures, and enables the development of principled evaluation tools. Namely, we want to understand how does a learned model, henceforth denoted by  $Q$ , compare to the target distribution  $P$ . Informally, to compute the precision we need to estimate how much probability  $Q$  assigns to regions of the space where  $P$  has high probability. Alternatively, to compute the recall we need to estimate how much probability  $P$  assigns to regions of the space that are likely under  $Q$ .

We start by developing an intuitive understanding of the problem with simple examples where the relationship between  $P$  and  $Q$  is easily understandable. Figure 1 illustrates the case where  $P$  and  $Q$  are uniform distributions with supports  $\text{supp}(P)$  and  $\text{supp}(Q)$ . To help with the exposition of our approach in the next section, we also introduce the distributions  $R_{\cup}$  and  $R_{\cap}$  which are uniform on the union and intersection of the supports of  $P$  and  $Q$  respectively. Then, the *loss in precision* can then be understood to be proportional to the measure of  $\text{supp}(Q) \setminus \text{supp}(R_{\cap})$  which corresponds to the "part of  $Q$  not covered by  $P$ ". Analogously, the *loss in recall* of  $Q$  w.r.t.  $P$  is proportional to the size of  $\text{supp}(P) \setminus \text{supp}(R_{\cap})$  which represents the "part of  $P$  not covered by  $Q$ ". Note that we can also write these sets as  $\text{supp}(R_{\cup}) \setminus \text{supp}(P)$  and  $\text{supp}(R_{\cup}) \setminus \text{supp}(Q)$  respectively. The precision and recall are then naturally maximized when  $P = Q$ . When the distributions are discrete, we expect tradeoffs similar to those in Figure 1b. In particular, the first column corresponds to  $Q$  which fails to model one of the modes of  $P$ , and the second column to a  $Q$  which has an "extra" mode. We would like our framework to mark these two failure modes as losses in recall and precision, respectively. The third column corresponds to  $P = Q$ , followed by a case where  $P$  and  $Q$  have disjoint support. Finally, for the last two columns, a possible precision-recall tradeoff is illustrated.

While this intuition is satisfying for uniform and categorical distributions, it is unclear how to extend it to continuous distributions that might be supported on the complete space.

### 3 Divergence Frontiers

To formally extend these ideas to the general case, we will introduce an auxiliary distribution  $R$  that is constrained to be supported only on those regions where both  $P$  and  $Q$  assign high probability<sup>2</sup>. Informally, this should act as a generalization to the general case of  $R_{\cap}$ , which was the measure on the intersection of the supports of  $P$  and  $Q$ . Then, the *discrepancy* between  $P$  and  $R$  measures the space that is likely under  $P$  but not under  $R$ , which can be seen as loss in recall. Similarly, the discrepancy between  $Q$  and  $R$  quantifies the size of the space where  $Q$  assigns probability mass, but  $P$  does not, which we can be interpreted as a loss in recall.

Hence, we need both a mechanism to measure distances between distributions and means to constrain  $R$  to assign mass only where both  $P$  and  $Q$  do. For example, if  $P$  and  $Q$  are both mixtures of several components  $R$  should assign mass only to the components shared by both  $P$  and  $Q$ .

**A dual view** Alternatively, building on the observation from the previous section that both  $R_{\cup}$  and  $R_{\cap}$  can be used to define precision and recall, instead of modeling the intersection of  $P$  and  $Q$ , we can use an auxiliary distribution  $R$  to approximate the *union* of the high-probability regions of  $P$  and  $Q$ . Then, using a similar analogy as before, the distance between  $P$  and  $R$  should measure the loss in precision, while the distance between  $Q$  and  $R$  the loss in recall. In this case,  $R$  should give non-zero probability to any part of the space where either  $P$  or  $Q$  assign mass. When  $P$  and  $Q$  are both mixtures of several components,  $R$  has to be supported on the union of all mixture components.

As a result, the choice of the statistical divergence between  $P$ ,  $Q$  and  $R$  becomes paramount.

#### 3.1 Choice of Divergence

To be able to constrain  $R$  to assign probability mass only in those regions where  $P$  and  $Q$  do, we need a measure of discrepancy between distributions that penalizes differently under- and over-coverage. Even though the theory and concepts introduced in this paper extend to any such divergence, we will focus our attention to the family of Rényi divergences. They not only do exhibit such behavior, but their properties are also well-studied in the literature, which we can leverage to develop a deeper understanding of our approach, and in the design of efficient computational tools.

**Definition 1** (Rényi Divergence [17]). *Let  $P$  and  $Q$  be two measures such that  $Q$  is absolutely continuous with respect to  $P$ , i.e., any measure set with zero measure under  $P$  has also zero measure under  $Q$ . Then, the Rényi divergence of order  $\alpha \in (0, 1) \cup (1, \infty)$  is defined as*

$$D_{\alpha}(P, Q) = \frac{1}{\alpha - 1} \log \int \left( \frac{dP}{dQ} \right)^{\alpha - 1} dP, \quad (1)$$

where  $dP/dQ$  is the Radon-Nikodym derivative<sup>3</sup>.

The fact that Rényi divergences are sensitive to how the supports of  $P$  and  $Q$  relate to one another is already hinted by the constraint in the definition, which requires that  $\text{supp}(P) \subseteq \text{supp}(Q)$ . Furthermore, by increasing  $\alpha$  the divergence becomes “less forgiving” — for example if  $P$  and  $Q$  are Gaussians with deviations  $\sigma_P$  and  $\sigma_Q$ , we have that  $D_{\alpha}(P \parallel Q)$  increases faster as  $\alpha \rightarrow \infty$  when  $\sigma_Q$  drops below  $\sigma_P$ , while  $D_{\alpha}(Q \parallel P)$  grows with increasing  $\sigma_Q$  and  $\alpha \rightarrow \infty$ , which we illustrate in Figure 2. This is exactly the property that we need to be able to define meaningful concepts of precision and recall. For a detailed analysis we point the reader to Minka et al. [12].

Rényi divergences have been extensively studied in the literature and many of their properties are well-understood — for example, they are non-negative and zero only if the distributions are equal a.s., and increasing in  $\alpha$  [23]. Some of their orders are closely related to the Hellinger and  $\chi^2$  divergences, and it can be further shown that  $D_{\text{KL}}(P \parallel Q) = \int \log \left( \frac{dP}{dQ} \right) dP = \lim_{\alpha \rightarrow 1} D_{\alpha}(P \parallel Q)$ .

#### 3.2 Divergence Frontiers

Having defined a suitable discrepancy measure, we are ready to define the central objects which will play the role of precision-recall curves for arbitrary measures. To do so, we will not put hard

<sup>2</sup>This is in contrast to [20], who require  $P$  and  $Q$  to be mixtures with a shared component.

<sup>3</sup>Equal to the ratios of the densities of  $P$  and  $Q$  when they both exist.

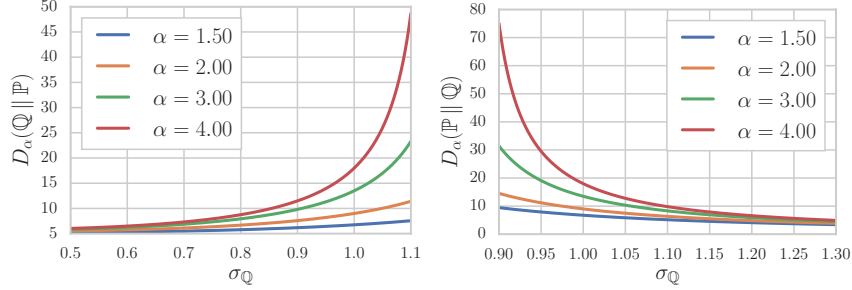


Figure 2: Rényi divergences between two measures quickly grow when the first argument assigns mass away from the high probability regions of its second argument. We evaluate the divergences in closed form where  $\mathbb{P}$  is a standard Normal [4].

constraints on  $R$ , but only softly enforce them. Namely, consider the case when we want  $R$  to model the intersection of the high likelihood regions of  $P$  and  $Q$ . Then, if it fails to do so, either  $D_\alpha(R \| P)$  or  $D_\alpha(R \| Q)$  will be significantly large. Similarly, unless  $R$  fails to assign large probabilities to the high likelihood regions of both  $P$  and  $Q$ , at least one of  $D_\alpha(P \| R)$  and  $D_\alpha(Q \| R)$  will be large. Thus, we will only consider those  $R$  that simultaneously minimize both divergences, which motivates the following definition.

**Definition 2** (Divergence frontiers). *For any two measures  $P$  and  $Q$ , any class of measures  $\mathcal{M}$  and any  $\alpha \geq 0$ , we define the exclusive realizable region as the set*

$$\mathcal{R}_\alpha^\cap(P, Q) = \{(D_\alpha(R, Q), D_\alpha(R, P)) \mid R \in \mathcal{M}\}, \quad (2)$$

*and the inclusive realizable region  $\mathcal{R}_\alpha^\cup(P, Q)$  by swapping the arguments of  $D_\alpha$  in (2). The exclusive and inclusive divergence frontiers are then defined as the maximal points of the corresponding realizable regions, i.e.,*

$$\mathcal{F}_\alpha^\cup(P, Q \mid \mathcal{M}) = \{(\pi, \rho) \in \mathcal{R}_\alpha^\cup(P, Q \mid \mathcal{M}) \mid \nexists (\pi', \rho') \in \mathcal{R}^\cup(P, Q) \text{ s.t. } \pi' < \pi \text{ and } \rho' < \rho\},$$

*and  $\mathcal{F}^\cap$  is defined analogously by replacing  $\mathcal{R}^\cup$  with  $\mathcal{R}^\cap$ .*

In other words, we want to compute the Pareto frontiers of the multi-objective optimization problem with the divergence minimization objectives  $f_1(R) = D_\alpha(R \| Q)$ ,  $f_2(R) = D_\alpha(R \| P)$  (exclusive), and  $f_3(R) = D_\alpha(Q \| R)$ ,  $f_4(R) = D_\alpha(P \| R)$  (inclusive), respectively. In machine learning such divergence minimization problems often appear in approximate inference. Interestingly,  $f_1$  and  $f_2$  are the central object one minimizes in variational inference (VI) [24, §5][9], while  $f_3$  and  $f_4$  are exactly the objectives in expectation propagation (EP) [11, 12]. Hence, the problem of computing the frontiers can be seen as that of performing VI or EP with two target distributions instead of one.

## 4 Computing the Frontiers

Having defined the frontiers, we now turn to the problem of their computation. Remember that to compute the inclusive frontier we have to characterize the set of all pairs  $(D_\alpha(R \| P), D_\alpha(R \| Q))$  which are not strictly dominated. To solve this multi-objective optimization problem we will linearly scalarize it by computing

$$\gamma(\lambda) = \arg \min_R \lambda D_\alpha(R \| Q) + (1 - \lambda) D_\alpha(R \| P), \quad (3)$$

for varying  $\lambda \in [0, 1]$ , and plug  $\gamma(\lambda)$  back in the divergences. Even though this approach does not in general guarantee that we will obtain the frontier, we show that it is indeed the case in our setting. Furthermore, problem (3) is known as the *barycenter problem* and has closed-form solutions for many classes of distributions, which we will make use of. The exclusive case will be treated analogously.

### 4.1 Discrete Measures

Let us first consider the discrete case, when the distributions take on one of  $n$  values. To simplify the discussion, we represent the distributions as vectors in the simplex  $\Delta = \{\boldsymbol{\mu} \in [0, 1]^n \mid \mathbf{1}^\top \boldsymbol{\mu} = 1\}$ ,

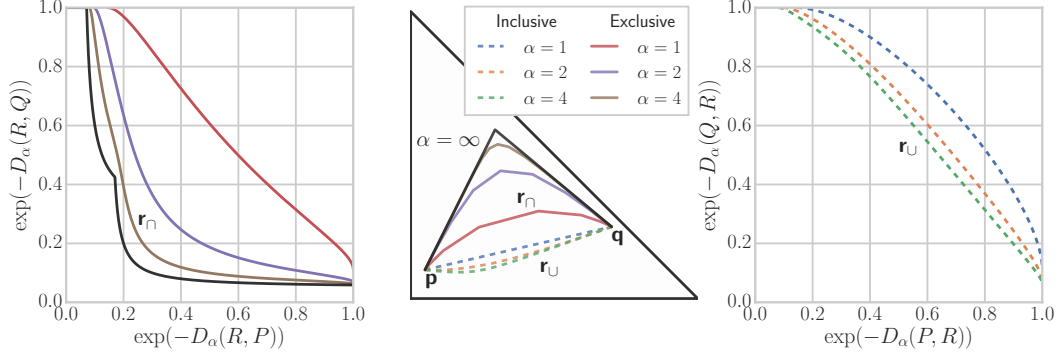


Figure 3: Illustration of the algorithm computing the discrete frontiers. In the middle panel we show two measures  $\mathbf{p}$  and  $\mathbf{q}$  on the probability simplex, together with the barycentric paths  $\gamma(\lambda)$  between them for various  $\alpha$ . These paths in turn generate the inclusive (right) and exclusive (left) frontiers. The limiting exclusive case  $\alpha = \infty$  coincides with the precision-recall curve from [20] (cf. §5).

and use  $\mathbf{p} \in \Delta$  for  $P$  and  $\mathbf{q} \in \Delta$  for  $Q$ . The vectors  $\gamma(\lambda)$  for the exclusive and inclusive case can be analytically computed [14, III], which results in the following computational scheme.

**Proposition 1.** *For any two discrete measures  $\mathbf{p}$  and  $\mathbf{q}$  in the probability simplex and any  $\alpha \geq 0$ , the forward and backward divergence frontiers can be computed as follows:*

i) *Exclusive: define the curve  $\gamma: [0, 1] \rightarrow \Delta$  by  $[\gamma(\lambda)]_i \propto (\lambda q_i^{1-\alpha} + (1-\lambda)p_i^{1-\alpha})^{1/(1-\alpha)}$ . Then,*

$$\mathcal{F}^\cap_\alpha(\mathbf{p}, \mathbf{q} \mid \Delta) = \{(D_\alpha(\gamma(\lambda), \mathbf{p}), D_\alpha(\gamma(\lambda), \mathbf{q})) \mid \lambda \in [0, 1]\}.$$

ii) *Inclusive: define the curve  $\gamma: [0, 1] \rightarrow \Delta$  by  $[\gamma(\lambda)]_i \propto (\lambda q_i^\alpha + (1-\lambda)p_i^\alpha)^{1/\alpha}$ . Then,*

$$\mathcal{F}^\cup_\alpha(\mathbf{p}, \mathbf{q} \mid \Delta) = \{(D_\alpha(\mathbf{p}, \gamma(\lambda)), D_\alpha(\mathbf{q}, \gamma(\lambda))) \mid \lambda \in [0, 1]\}.$$

Conceptually, to compute the frontier we walk along the path  $\gamma_\alpha$  from  $\mathbf{p}$  to  $\mathbf{q}$ , and at each point we compute the distances to  $\mathbf{p}$  and  $\mathbf{q}$  as measured by  $D_\alpha$ . We illustrate this in Figure 3.

## 4.2 Continuous Measures

The computation of the frontier for continuous distributions presents several obstacles that do not exist in the discrete case. Namely, even if we have access to the densities of  $P$  and  $Q$ , characterizing their frontiers can be arduous — it is not obvious how to parameterize  $R$ , and furthermore optimizing and evaluating the divergences can be challenging. Fortunately, for the *exponential family*, which includes many commonly used distributions such as Gaussian, Lognormal, and Exponential, these frontiers can be efficiently computed for  $\alpha = 1$  (i.e., the KL divergence).

**Definition 3** (Exponential family [24, §3.2]). *The exponential family over a domain  $\mathcal{X}$  for a sufficient statistic  $\nu: \mathcal{X} \rightarrow \mathbb{R}^m$  is the set of all distributions of the form*

$$P(x \mid \boldsymbol{\theta}) = \exp(\boldsymbol{\theta}^\top \nu(x) - A(\boldsymbol{\theta})), \quad (4)$$

where  $\boldsymbol{\theta}$  is the parameter vector, and  $A(\boldsymbol{\theta})$  is the log-partition function normalizing the distribution.

Importantly, the KL divergence between two distributions in the exponential family with parameters  $\boldsymbol{\theta}$  and  $\boldsymbol{\theta}'$  can be computed in closed form as the following Bregman divergence [24, §5.2.2]

$$D_{\text{KL}}(P(\cdot \mid \boldsymbol{\theta}) \parallel P(\cdot \mid \boldsymbol{\theta}')) = A(\boldsymbol{\theta}') - A(\boldsymbol{\theta}) - \nabla A(\boldsymbol{\theta})^\top (\boldsymbol{\theta}' - \boldsymbol{\theta}),$$

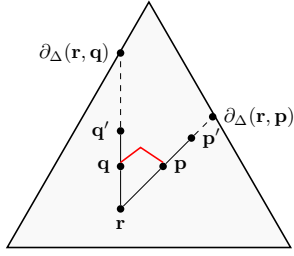
which we shall denote as  $D_{\text{KL}}(\boldsymbol{\theta} \parallel \boldsymbol{\theta}')$ . We can now show how to compute the frontier.

**Proposition 2.** *Let  $\mathcal{M}$  be an exponential family with log-partition function  $A$ . Let  $P$  and  $Q$  be elements in  $\mathcal{M}$  with parameters  $\boldsymbol{\theta}_P$  and  $\boldsymbol{\theta}_Q$ . Then,*

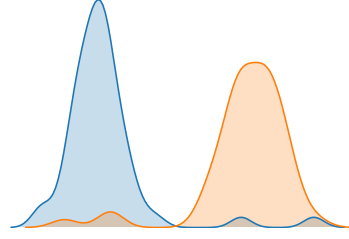
- *Inclusive: If we define  $\gamma(\lambda) = (\nabla A)^{-1}(\lambda \nabla A(\boldsymbol{\theta}_P) + (1-\lambda) \nabla A(\boldsymbol{\theta}_Q))$ , then*  

$$\mathcal{F}^\cup_1(P, Q \mid \mathcal{M}) = \{(D_{\text{KL}}(\boldsymbol{\theta}_P \parallel \gamma(\lambda)), D_{\text{KL}}(\boldsymbol{\theta}_Q \parallel \gamma(\lambda))) \mid \lambda \in [0, 1]\}.$$
- *Exclusive: If we define  $\gamma(\lambda) = \lambda \boldsymbol{\theta}_P + (1-\lambda) \boldsymbol{\theta}_Q$ , then*  

$$\mathcal{F}^\cap_1(P, Q \mid \mathcal{M}) = \{(D_{\text{KL}}(\gamma(\lambda) \parallel \boldsymbol{\theta}_P), D_{\text{KL}}(\gamma(\lambda) \parallel \boldsymbol{\theta}_Q)) \mid \lambda \in [0, 1]\}.$$



(a) Exact geometric characterization of PRD [20].



(b) A failure case for [8].

Figure 4: (a) The probability simplex with all points involved in the definition of PRD [20]. For these fixed measures  $\mathbf{p}$ ,  $\mathbf{q}$  and  $\mathbf{r}$ , the points  $\mathbf{p}'$  and  $\mathbf{q}'$  must lie on the rays  $\mathbf{r} \rightarrow \mathbf{q}$  and  $\mathbf{r} \rightarrow \mathbf{p}$  respectively. The optimal precision and recall are obtained when  $\mathbf{q}'$  and  $\mathbf{r}'$  lie on the boundary. To compute the frontier we have to consider *only those*  $\mathbf{r}$  which lie on the geodesic between  $\mathbf{q}$  and  $\mathbf{p}$ , shown as the red curve. Figure (b) shows a case where the metric defined by [8] results in essentially perfect precision and recall. Arguably, in this case the precision and recall should both be low.

## 5 Connections to Related Work

We will now show that the two most prominent definitions of precision and recall are special cases of the presented framework.

**The limiting case of  $\alpha \rightarrow 0$**  Rather than computing tradeoff curves, Kynkäänniemi et al. [8] focus only on computing  $P(\text{supp}(Q))$  and  $Q(\text{supp}(P))$ , and estimate the supports using a union of  $k$ -nearest neighbourhood balls. This is indeed a special case of our framework, as [23, Thm. 4]  $\lim_{\alpha \rightarrow 0} D_{\alpha}(P \| Q) = -\log Q(\text{supp}(P))$ . One drawback of this approach is that all regions where  $P$  and  $Q$  place any mass are considered equal. Hence, for any two measures with the same support this metric assigns perfect precision and recall (see Figure 4b).

**The limiting case of  $\alpha \rightarrow \infty$**  We will now show that [20] corresponds to the case where  $\alpha \rightarrow \infty$ . In particular, Sajjadi et al. [20] write both  $P$  and  $Q$  as mixtures with a shared component that should capture the space to which both assign high likelihood, and which can be used to formalize the notions of precision and recall for distributions.

**Definition 4** ([20, Def. 1]). *For  $\pi, \rho \in (0, 1]$ , the probability distribution  $Q$  has precision  $\pi$  at recall  $\rho$  w.r.t.  $P$  if there exist distributions  $R, P', Q'$  such that*

$$P = \rho R + (1 - \rho)P', \text{ and } Q = \pi R + (1 - \pi)Q'. \quad (5)$$

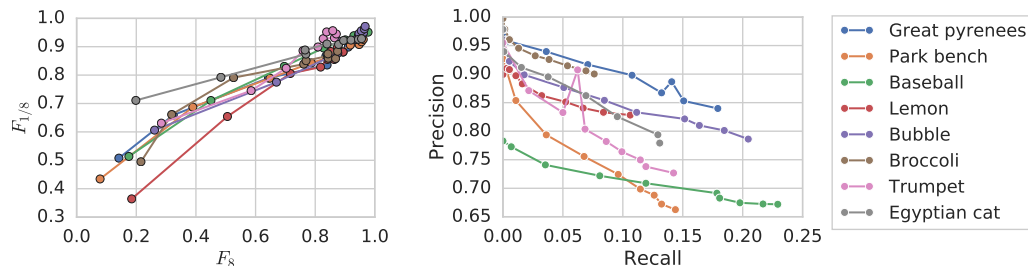
*The union of  $\{(0, 0)\}$  and all realizable pairs  $(\pi, \rho)$  will be denoted by  $\text{PRD}(P, Q)$ .*

Even though the divergence frontiers formalized in this work might seem unrelated to this definition, there is a clear connection between them, which we now establish. As [20] targets discrete measures, let us treat the distributions as vectors in the probability simplex  $\Delta$  and use  $\mathbf{p} \in \Delta$  for  $P$  and  $\mathbf{q} \in \Delta$  for  $Q$ . We need to consider three additional distributions to compute  $\text{PRD}(\mathbf{p}, \mathbf{q})$ :  $\mathbf{r}$ , and the per-distribution mixtures  $\mathbf{p}'$  and  $\mathbf{q}'$ . These distributions are arranged as shown in Figure 4. Because  $\mathbf{r}$ ,  $\mathbf{p}$  and  $\mathbf{p}'$  are co-linear and  $\mathbf{p} = \rho \mathbf{r} + (1 - \rho)\mathbf{p}'$ , we have that the recall obtained for this configuration is  $\|\mathbf{p} - \mathbf{p}'\|/\|\mathbf{r} - \mathbf{p}'\|$ . Similarly, the precision  $\pi$  can be easily seen to be equal to  $\|\mathbf{q} - \mathbf{q}'\|/\|\mathbf{r} - \mathbf{q}'\|$ . Most importantly, we can only increase both  $\rho$  and  $\pi$  if we move  $\mathbf{p}'$  and  $\mathbf{q}'$  along the rays  $\mathbf{r} \rightarrow \mathbf{p}$  and  $\mathbf{r} \rightarrow \mathbf{q}$ , respectively. Specifically, the maximal recall  $\rho^*$  and precision  $\pi^*$  for this fixed  $\mathbf{r}$  are obtained when  $\mathbf{p}'$  and  $\mathbf{q}'$  are as far as possible from  $\mathbf{r}$ , i.e., when they lie on the boundary  $\partial\Delta$ . To formalize this, let us denote for any  $\mathbf{a}, \mathbf{b}$  in  $\Delta$  by  $\partial_{\Delta}(\mathbf{a}, \mathbf{b})$  the point along the ray  $\mathbf{a} \rightarrow \mathbf{b}$  that intersects the boundary of  $\Delta$ . Then, the maximal  $\pi$  and  $\rho$  are achieved for  $\mathbf{p}' = \partial_{\Delta}(\mathbf{r}, \mathbf{p})$  and  $\mathbf{q}' = \partial_{\Delta}(\mathbf{r}, \mathbf{q})$ . Perhaps surprisingly, these best achievable precision and recall have been already studied in geometry and have very remarkable properties, as they give rise to a weak metric.

**Definition 5** ([16, Def. 2.1]). *The Funk weak metric  $F_{\Delta}: \Delta^2 \rightarrow [0, \infty)$  on  $\Delta$  is defined by*

$$F_{\Delta}(\mathbf{p}, \mathbf{p}) = 0 \text{ and } F_{\Delta}(\mathbf{p}, \mathbf{q}) = \log(\|\mathbf{p} - \partial_{\Delta}(\mathbf{p}, \mathbf{q})\|/\|\mathbf{q} - \partial_{\Delta}(\mathbf{p}, \mathbf{q})\|).$$

Furthermore, we have that the Funk metric coincides with a limiting Rényi divergence.



(a) Precision ( $F_{1/8}$ ) and recall ( $F_8$ ) from [20].

(b) Precision and recall estimated using [8].

Figure 5: Figure (a) illustrates the main issue with the approach of Sajjadi et al. [20] – if the quantization is not carefully performed, it seems that truncation improves both precision and recall. On the other hand, panel (b) demonstrates that the estimator from [8] (notwithstanding the fundamental issues outlined in Section 5) performs well in practice.

**Proposition 3** ([15, Ex. 4.1],[23, Thm. 6]). *For any  $\mathbf{p}, \mathbf{q}$  in the probability simplex  $\Delta$ , we have that*

$$F_{\Delta}(\mathbf{p}, \mathbf{q}) = \lim_{\alpha \rightarrow \infty} D_{\alpha}(\mathbf{p} \parallel \mathbf{q}) = \log \max_{i=1}^n p_i/q_i$$

This immediately implies the following connection between the set of maximal points in  $\text{PRD}(P, Q)$ , which we shall denote by  $\overline{\text{PRD}}(P, Q)$  and  $\mathcal{F}_{\infty}^{\cap}(\mathbf{p}, \mathbf{q})$ . In other words, the maximal points in PRD coincide with one of the exclusive frontiers we have introduced.

**Proposition 4.** *For any distributions  $P, Q$  on  $\{1, 2, \dots, n\}$  it holds that*

$$\overline{\text{PRD}}(P, Q) = \{(e^{-\pi}, e^{-\rho}) \mid (\rho, \pi) \in \mathcal{F}_{\infty}^{\cap}(P, Q)\}.$$

Furthermore, the fact that  $D_{\infty}$  is a weak metric implies that, in contrast to the  $\alpha < \infty$  case, the triangle inequality holds [16, Thm. 7.1]. As a result, we can make an even stronger claim — the path traced-out by the distributions  $\mathbf{r}$  that generate the frontier is the *shortest in the corresponding geometry*.

**Proposition 5.** *Define the curve  $\gamma(\lambda): [\min_i \frac{q_i}{p_i}, \max_i \frac{q_i}{p_i}] \rightarrow \Delta$  as  $[\gamma(\lambda)]_i \propto \min\{p_i, q_i/\lambda\}$ . Then,*

$$\mathcal{F}_{\infty}^{\cap}(\mathbf{p}, \mathbf{q}) = \{(D_{\infty}(\gamma(\lambda) \parallel \mathbf{p}), D_{\infty}(\gamma(\lambda) \parallel \mathbf{q})) \mid \lambda \in [\min_i \frac{q_i}{p_i}, \max_i \frac{q_i}{p_i}]\},$$

and, moreover,  $\gamma(\lambda)$  is geodesic, i.e., it evaluates at the endpoints to  $\mathbf{p}$  and  $\mathbf{q}$ , and for any  $\lambda$

$$F_{\Delta}(\mathbf{p}, \mathbf{q}) = F_{\Delta}(\mathbf{p}, \gamma(\lambda)) + F_{\Delta}(\gamma(\lambda), \mathbf{q}).$$

Finally, we note that the idea of precision and recall for generative models based on distances to the corresponding manifolds first appeared in Lucic et al. [10], but was only applicable for synthetic data.

## 6 Practical Considerations and Insights

**Main Design Choices** In practice, when we are tasked with the problem of evaluating a generative model, we typically only have access to samples from the target distribution  $P$  and the model  $Q$ , and optionally also the density of  $Q$ . There are at least two approaches one can undertake when applying the methods developed in this paper to generate precision-recall curves. We would like to point out that in the case of image synthesis, the comparison is typically not done in the original high-dimensional image space, but (as done in [20, 8, 6]) in feature spaces where distances are expected to correlate more strongly with perceptual difference.

The first strategy is to discretize the data, as done in [20], and then apply the methods from Section 4.1. Even though in the limit this will converge to the continuous  $\alpha$  divergence [23, Thm. 2], there may be several issues with this approach — if clustering is used for quantization, as done in [20], the results might strongly depend on the clustering quality, and additional hyperparameters have to be tuned.

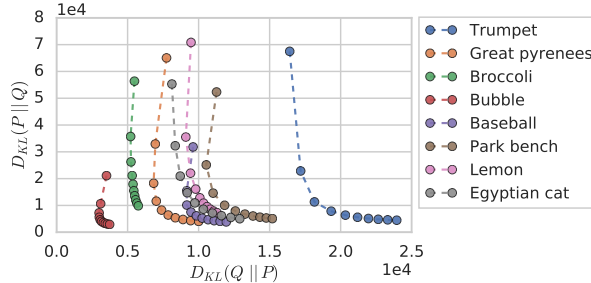


Figure 6: A simple strategy to recover the expected precision-recall tradeoff is to simply fit multivariate Gaussians to the real and fake data separately, and evaluate the end-points of  $\mathcal{F}_{\text{KL}}^{\Omega}(P, Q)$ . This simple approach which amounts to evaluating  $D_{\text{KL}}(Q \parallel P)$  (sensitive to precision losses) and  $D_{\text{KL}}(P \parallel Q)$  (sensitive to recall losses) decreases as we increase the truncation parameter from 0.1 to 1.

The second strategy is to fit a parametric model (from the exponential family) to samples from  $P$  and  $Q$  separately and apply the methods from Section 4.2. While this might seem simplistic, exactly this approach has been shown to work well for evaluating generative models using the FID score [6].

**Implications of the Design Choices** While it might seem that these design choices do not have a major impact on the qualitative interpretation of the results, their impact may be critical. Kynkäänniemi et al. [8] have already uncovered a counter-intuitive behavior of PRD resulting from quantization issues. Namely, they consider a class-conditional BigGAN model [3] trained on  $256 \times 256$  images from ImageNet [19]. The generator was trained to map a standard multivariate Gaussian variable  $Z$  to a distribution over high-dimensional natural images. To control the distribution at the output of the generator, Brock et al. [3] explored various *truncation strategies*. In particular, instead of sampling  $Z$  from a Gaussian as done during training, they re-sample all entries of the sampled vector  $Z$  that exceed (in absolute value) some fixed truncation threshold  $\tau$ . The idea is that low values of  $\tau$  should yield more visually pleasing samples at a cost of sample diversity, while the behavior should reverse for larger thresholds. As a result, as one increases the truncation parameter  $\tau$ , the precision should decrease and the recall should increase. In our experiments, we varied  $\tau$  ranging from 0.1 to 1.0 in increments of 0.1. Following [8, 3], we compare the images in the feature space of the second fully connected layer of a VGG network trained on ImageNet [22]. For each class we used 50000 generated samples and 1300 real ones (as many as there are in the dataset). As shown in Figure 5a and observed by Kynkäänniemi et al. [8], when measuring precision and the recall using the PRD metric [20], one seems to be able to improve both by truncation. On the other hand, the estimator from [8], shown in Figure 5b, can correctly identify the expected behavior in that particular setting, despite the fundamental issues illustrated in Section 5.

One can side-step these issues by instantiating our framework for the case of  $\alpha = 1$  (the KL-divergence) and approximate the real and fake data separately with multivariate Gaussians. By evaluating the end-points of  $\mathcal{F}_{\text{KL}}(P, Q)$ , which corresponds to evaluating the KL divergence between these two Gaussians (seen by setting  $R = P$  and  $R = Q$  in Def. 2), one observes the expected behavior. Namely, as shown in Figure 6,  $D_{\text{KL}}(Q \parallel P)$  (sensitive to precision losses) increases while  $D_{\text{KL}}(P \parallel Q)$  (sensitive to recall losses) decreases as we increase the truncation parameter. Hence, when one approximates the frontiers from finite samples, extra care has to be taken — for example, while discretization might make sense in the presence of multi-modality, fitting exponential families could be more suitable in capturing the tails of the distributions.

## 7 Conclusion

We developed a framework for comparing distributions via the Pareto frontiers of information divergences, and fully characterized them using efficient computational algorithms for a large family of distributions. We recovered previous approaches as special cases, and thus provided a novel perspective on their definitions and corresponding algorithms. Furthermore, we believe that we have also opened many interesting research questions related to classical approximate inference methods — can we use different divergences or extend the algorithms to even richer model families, and how to identify the correct approach for approximating the frontiers when we only have access to samples.



## References

- [1] Arindam Banerjee, Srujana Merugu, Inderjit S Dhillon, and Joydeep Ghosh. Clustering with Bregman divergences. *Journal of Machine Learning Research*, 2005.
- [2] Stephen Boyd and Lieven Vandenbergh. *Convex optimization*. Cambridge University Press, 2004.
- [3] Andrew Brock, Jeff Donahue, and Karen Simonyan. Large scale GAN training for high fidelity natural image synthesis. *International Conference on Learning Representations*, 2019.
- [4] Manuel Gil, Fady Alajaji, and Tamas Linder. Rényi divergence measures for commonly used univariate continuous distributions. *Information Sciences*, 2013.
- [5] Ian Goodfellow, Jean Pouget-Abadie, Mehdi Mirza, Bing Xu, David Warde-Farley, Sherjil Ozair, Aaron Courville, and Yoshua Bengio. Generative Adversarial Nets. *Advances in Neural Information Processing Systems*, 2014.
- [6] Martin Heusel, Hubert Ramsauer, Thomas Unterthiner, Bernhard Nessler, and Sepp Hochreiter. GANs trained by a two time-scale update rule converge to a local Nash equilibrium. *Advances in Neural Information Processing Systems*, 2017.
- [7] Diederik P Kingma and Max Welling. Auto-encoding Variational Bayes. *International Conference on Learning Representations*, 2014.
- [8] Tuomas Kynkäänniemi, Tero Karras, Samuli Laine, Jaakko Lehtinen, and Timo Aila. Improved Precision and Recall Metric for Assessing Generative Models. *arXiv preprint arXiv:1904.06991*, 2019.
- [9] Yingzhen Li and Richard E Turner. Rényi divergence variational inference. *Advances in Neural Information Processing Systems*, 2016.
- [10] Mario Lucic, Karol Kurach, Marcin Michalski, Sylvain Gelly, and Olivier Bousquet. Are GANs Created Equal? A Large-Scale Study. *Advances in Neural Information Processing Systems*, 2018.
- [11] Thomas P Minka. Expectation propagation for approximate Bayesian inference. *Conference on Uncertainty in artificial intelligence*, 2001.
- [12] Tom Minka et al. Divergence measures and message passing. Technical report, Technical report, Microsoft Research, 2005.
- [13] Frank Nielsen and Richard Nock. On the centroids of symmetrized Bregman divergences. *arXiv preprint arXiv:0711.3242*, 2007.
- [14] Frank Nielsen and Richard Nock. The dual Voronoi diagrams with respect to representational Bregman divergences. *International Symposium on Voronoi Diagrams*, 2009.
- [15] Athanase Papadopoulos and Marc Troyanov. From Funk to Hilbert Geometry. *arXiv preprint arXiv:1406.6983*, 2014.
- [16] Athanase Papadopoulos and Sumio Yamada. The Funk and Hilbert geometries for spaces of constant curvature. *Monatshefte für Mathematik*, 2013.
- [17] Alfréd Rényi. On measures of information and entropy. *Berkeley Symposium on Mathematics, Statistics and Probability*, 1961.
- [18] Danilo Jimenez Rezende, Shakir Mohamed, and Daan Wierstra. Stochastic backpropagation and approximate inference in deep generative models. *arXiv preprint arXiv:1401.4082*, 2014.
- [19] Olga Russakovsky, Jia Deng, Hao Su, Jonathan Krause, Sanjeev Satheesh, Sean Ma, Zhiheng Huang, Andrej Karpathy, Aditya Khosla, Michael Bernstein, Alexander C. Berg, and Li Fei-Fei. ImageNet Large Scale Visual Recognition Challenge. *International Journal of Computer Vision*, 2015.
- [20] Mehdi SM Sajjadi, Olivier Bachem, Mario Lucic, Olivier Bousquet, and Sylvain Gelly. Assessing generative models via precision and recall. *Advances in Neural Information Processing Systems*, 2018.
- [21] Tim Salimans, Ian Goodfellow, Wojciech Zaremba, Vicki Cheung, Alec Radford, and Xi Chen. Improved techniques for training GANs. *Advances in Neural Information Processing Systems*, 2016.

- [22] Karen Simonyan and Andrew Zisserman. Very deep convolutional networks for large-scale image recognition. *arXiv preprint arXiv:1409.1556*, 2014.
- [23] Tim Van Erven and Peter Harremo. Rényi divergence and kullback-leibler divergence. *IEEE Transactions on Information Theory*, 2014.
- [24] Martin J Wainwright, Michael I Jordan, et al. Graphical models, exponential families, and variational inference. *Foundations and Trends® in Machine Learning*, 2008.

## A Proofs

*Proof of Proposition 4.* Even though this result follows clearly from the discussion just above the claim, we provide it for completeness. Namely, let  $(\pi, \rho) \in \text{PRD}$  be generated for some  $\mathbf{p}, \mathbf{q}, \mathbf{r}$ . Based on the argument below Definition 4 it follows that it must be equal to  $(\pi, \rho) = (e^{-F_\Delta(\mathbf{r}, \mathbf{q})}, e^{-F_\Delta(\mathbf{r}, \mathbf{p})})$ . Then, the pair  $(\pi, \rho)$  is maximal in PRD iff  $(F_\Delta(\mathbf{r}, \mathbf{p}), F_\Delta(\mathbf{r}, \mathbf{q}))$  is minimal in  $\mathcal{R}_\infty^\cap(P, Q)$ , i.e., iff  $(F_\Delta(\mathbf{r}, \mathbf{p}), F_\Delta(\mathbf{r}, \mathbf{q})) \in \mathcal{F}_\infty^\cap(P, Q)$ .  $\square$

*Proof of Proposition 5.* If we also include the normalizer of  $\gamma(\lambda)$ , we have that

$$[\gamma(\lambda)]_i = \min\{p_i, q_i/\lambda\}/\beta(\lambda), \text{ where } \beta(\lambda) = \sum_{i=1}^n \min\{p_i, q_i/\lambda\}.$$

The end-point condition is easy to check, namely

$$\begin{aligned} [\gamma \min\{q_j/p_j\}]_i &= \min\{p_i, \frac{q_i}{\min_j\{q_j/p_j\}}\}/\beta(\lambda) = p_i/\beta(\lambda) = p_i, \text{ and} \\ [\gamma(\min\{q_j/p_j\})]_i &= \min\{p_i, \frac{q_i}{\max_j\{q_j/p_j\}}\}/\beta(\lambda) = q_i/\beta(\lambda) = q_i. \end{aligned}$$

Let us now show that  $\log \beta(\lambda) = -F_\Delta(\gamma(\lambda), \mathbf{q})$ . The right hand side can be re-written as

$$F_\Delta(\gamma(\lambda), \mathbf{p}) = \log \max_i \frac{\min\{p_i, q_i/\lambda\}/\beta(\lambda)}{p_i} = -\log \beta(\lambda) + \log \max_i \min\{1, \frac{q_i}{p_i\lambda}\}.$$

Note that the term inside the log is not one only if  $q_i/p_i < \lambda$  for all  $i$ , which can happen only if  $\lambda > \max_i \frac{q_i}{p_i}$ , which is outside the domain of  $\gamma$ . Similarly,

$$\begin{aligned} F_\Delta(\gamma(\lambda), \mathbf{q}) &= \log \max_i \frac{\min\{p_i, q_i/\lambda\}/\beta(\lambda)}{q_i} \\ &= -\log \beta(\lambda) + \log \max_i \min\{\frac{p_i}{q_i}, 1/\lambda\} \\ &= -\log \beta(\lambda)\lambda + \log \max_i \min\{\frac{\lambda p_i}{q_i}, 1\}. \end{aligned}$$

The claim follows because  $\alpha(\lambda) = \lambda\beta(\gamma)$ , and by noting that the maximum inside the logarithm is strictly less than one only if for all  $i$  it holds that  $\lambda < \frac{q_i}{p_i}$ , which is outside the domain of  $\gamma$ .

Finally, let us show the geodesy of the curve.

$$\begin{aligned} F_\Delta(\mathbf{p}, \boldsymbol{\mu}^*(\lambda)) + F_\Delta(\boldsymbol{\mu}^*(\lambda), \mathbf{q}) &= \log \max_i \frac{p_i}{\min\{p_i, q_i/\lambda\}/\beta(\lambda)} + \log \max_i \frac{\min\{p_i, q_i/\lambda\}/\beta(\lambda)}{q_i} \\ &= \max_i \log \max\{\log \frac{\lambda p_i}{q_i}, 1\} + \max_i \log \min\{\frac{p_i}{q_i}, \frac{1}{\lambda}\} \end{aligned}$$

- *Case (i):*  $\lambda \geq \max_i \frac{q_i}{p_i}$ . Then,  $\frac{\lambda p_i}{q_i} \lambda \geq 1$ , so that the first term will be equal to  $\log \lambda + \log \max_i \frac{p_i}{q_i}$ . Similarly,  $\lambda^{-1} \leq \frac{p_i}{q_i}$ , so that the second term is equal to  $-\log \lambda$ , and the claimed equality is satisfied.

- *Case (ii):*  $\lambda < \max_i \frac{q_i}{p_i}$ . Note that

$$\begin{aligned} & \max_i \log \max\left\{\log \frac{\lambda p_i}{q_i}, 1\right\} + \max_i \log \min\left\{\frac{p_i}{q_i}, \frac{1}{\lambda}\right\} = \\ & \max_i \log \lambda \max\left\{\log \frac{p_i}{q_i}, 1/\lambda\right\} + \max_i \log \frac{1}{\lambda} \min\left\{\frac{p_i \lambda}{q_i}, 1\right\}, \end{aligned}$$

so that the problem is symmetric if we parametrize with  $\lambda' = \lambda^{-1}$  and the argument from above holds. □

*Proof of Proposition 1. Case (i)* Remember that we want to minimize  $\mathbf{r} \rightarrow D_\alpha(\mathbf{r} \parallel \mathbf{p})$  and  $\mathbf{r} \rightarrow D_\alpha(\mathbf{r} \parallel \mathbf{q})$ . Instead of minimizing the Rényi divergences  $\frac{1}{\alpha-1} \log \sum_{i=1}^n (r_i/q_i)^{\alpha-1} r_i$ , we can alternatively minimize the  $\alpha$ -divergences  $\frac{4}{\alpha^2-1} \sum_{i=1}^n (r_i/p_i)^{\alpha-1} r_i$  as they are monotone functions of each other. As the  $\alpha$  divergence is an  $f$ -divergence (see e.g. [14, C]), it follows that it is jointly convex in both arguments. Hence the Pareto frontier can be computed using the linearly scalarized problem (for a proof see [2, §4.7.3]). The fact that the solution to  $\lambda D_\alpha(\mathbf{r} \parallel \mathbf{p}) + (1-\lambda) D_\alpha(\mathbf{r} \parallel \mathbf{q})$  is given by  $[\mathbf{r}(\lambda)]_i \propto (p_i + q_i)^{-1}$  is proven in [14, (12)]. *Case (ii)* This case follows analogously as above as the  $f$ -divergence is jointly convex. The formula for the barycenter can be found in [14, (13)]. □

*Proof of Proposition 2.* The proof follows the same argument of Nielsen and Nock [13, §2], the main difference that we also discuss about Pareto optimality, while in the [13] the authors only discuss the barycenter problem. Let us denote for any convex continuously differentiable function  $G: \mathbb{R}^d \rightarrow \mathbb{R}$  by  $B_G: \mathbb{R}^d \times \mathbb{R}^d \rightarrow \mathbb{R}$  the Bregman divergence generated by  $G$ , i.e.,

$$B_G(\mathbf{x}, \mathbf{y}) = F(\mathbf{x}) - F(\mathbf{y}) - \nabla F(\mathbf{y})^\top (\mathbf{x} - \mathbf{y}).$$

In the inclusive case, we want to minimize the objectives  $\boldsymbol{\theta}_R \rightarrow D_\alpha(\boldsymbol{\theta}_P \parallel \boldsymbol{\theta}_R)$  and  $\boldsymbol{\theta}_R \rightarrow D_\alpha(\boldsymbol{\theta}_Q \parallel \boldsymbol{\theta}_R)$  over  $\boldsymbol{\theta}_R$ . In terms of Bregman divergences, we want to minimize  $B_A(\boldsymbol{\theta}_R, \boldsymbol{\theta}_P)$  and  $B_A(\boldsymbol{\theta}_R, \boldsymbol{\theta}_Q)$ . Because Bregman divergences are convex in their first argument, as in the proof of Proposition 1 we can only consider the solutions to the linearly scalarized objective

$$\lambda B_A(\boldsymbol{\theta}_R, \boldsymbol{\theta}_P) + (1-\lambda) B_A(\boldsymbol{\theta}_R, \boldsymbol{\theta}_Q),$$

whose solution is known (see e.g. [1]) to be equal to  $\boldsymbol{\theta}_R^*(\lambda) = \lambda \boldsymbol{\theta}_P + (1-\lambda) \boldsymbol{\theta}_Q$ , which we had to show. The exclusive case follows from the same argument using the fact that  $B_A(\boldsymbol{\theta}, \boldsymbol{\theta}') = B_{A^*}(\nabla A(\boldsymbol{\theta}'), \nabla A(\boldsymbol{\theta}))$  and that  $\nabla A^* = (\nabla A)^{-1}$  [24, Prop. B.2]. □